

## Band structures of rare-gas solids within the *GW* approximation

S. Galamić-Mulaomerović and C. H. Patterson

Department of Physics and Center for Scientific Computation, University of Dublin, Trinity College, Dublin 2, Ireland

(Received 21 September 2004; revised manuscript received 15 December 2004; published 6 May 2005)

Band structures for solid rare gases (Ne, Ar) have been calculated using the *GW* approximation. All electron and pseudopotential *ab initio* calculations were performed using Gaussian orbital basis sets and the dependence of particle-hole gaps and electron affinities on basis set and treatment of core electrons is investigated. All electron *GW* calculations have a smaller particle-hole gap than pseudopotential *GW* calculations by up to 0.2 eV. Quasiparticle electron and hole excitation energies, valence bandwidths and electron affinities are generally in very good agreement with those derived from optical absorption and photoemission measurements.

DOI: 10.1103/PhysRevB.71.195103

PACS number(s): 71.20.-b, 78.20.Bh, 78.40.-q, 79.60.-i

### I. INTRODUCTION

Optical spectra and band structures of rare gas solids (RGS) have been studied, both experimentally and theoretically, for over 40 years. Their importance lies in the simplicity of their crystal structure, the nearly atomic character of valence states versus extended character of conduction states, and the fact that they have strong many-body effects in their optical spectra. They are an important testing ground for electronic structure methods and as electronic structure methods have developed, they have been applied to RGS. Early electronic structure studies included applications of density-functional theory,<sup>1-3</sup> (DFT), Hartree-Fock theory<sup>4-7</sup> (HFT), and self-interaction corrected DFT.<sup>8</sup> Some of these studies have included correlation effects in the band structure via many-body perturbation theory.<sup>1,2,5,7,9</sup>

In this paper we present results of *ab initio* all electron and pseudopotential many-body calculations of the band structures of solid Ne and Ar using Gaussian orbital basis sets. Band structures are calculated using the *GW* approximation<sup>10-13</sup> and the dependence of particle-hole gaps and electron affinities on basis set and treatment of core electrons is investigated. In another paper<sup>14</sup> we will present results of calculations of optical spectra of these solids using a Bethe-Salpeter formalism.<sup>9</sup> Calculations were performed in a Gaussian orbital basis using the EXCITON code,<sup>15</sup> which is interfaced to the CRYSTAL code.<sup>16</sup> Single-particle wave functions, energy eigenvalues, and matrix elements of the exchange-correlation potential from CRYSTAL are used by EXCITON to perform *GW* and exciton calculations. The principal parameters of the band structures of RGS, which have been obtained experimentally, are the particle-hole band gap  $E_G$ , the valence bandwidth  $W_V$ , and the electron affinity  $E_A$ . The particle-hole gap is the energy difference for particle and hole excitations at the conduction-band minimum and valence-band maximum. It has been obtained experimentally from absorption spectrum<sup>17</sup> and photoemission measurements.<sup>18,19</sup>

The *GW* approximation is a many-body perturbation theory and therefore contains corrections to a simpler, single-particle (SP) Hamiltonian. It was originally applied to semiconductors using a DFT Kohn-Sham Hamiltonian, a plane-wave basis set, and pseudopotential (PP) approximation for

core electrons<sup>12</sup> and was found to give excellent agreement with experiment for relatively narrow band-gap materials, such as Si, where DFT results in an indirect band gap that underestimates the experimental value by  $\sim 0.7$  eV.

All electron *GW* calculations have been performed recently for a variety of crystalline solids, including Si.<sup>20-24</sup> Most all electron *GW* calculations of indirect band gaps of Si<sup>20,22,23</sup> underestimate the experimental value of 1.17 eV by 0.2–0.3 eV. There has been some debate whether this is due to incompleteness of the basis<sup>25</sup> or explicit inclusion of the core electrons (all electron rather than PP approximation).<sup>20-23,26</sup> However, one self-consistent all electron *GW* calculation<sup>24</sup> finds excellent agreement with the experimental band gap in Si. In the present work we compare results for the RGS using both all electron and PP approximations for the core electrons.

The remainder of this paper is organized as follows: in Sec. II the *GW* formalism used here is outlined, in Sec. III results of *GW* band-structure calculations are compared to experiment and earlier *GW* calculations on Ne and Ar. Finally, conclusions are given in Sec. IV. The basis sets and their convergence are presented in the Appendix.

### II. GW APPROXIMATION

#### A. Quasiparticle energies

Conceptually, single electron and hole excitations are described by

$$H(\mathbf{r})\psi_m^{QP}(\mathbf{r}) + \int \Sigma(\mathbf{r}, \mathbf{r}', E)\psi_m^{QP}(\mathbf{r}')d\mathbf{r}' = \epsilon_m\psi_m^{QP}(\mathbf{r}). \quad (1)$$

The self-energy operator,  $\Sigma(\mathbf{r}, \mathbf{r}', E)$ , is non-Hermitian, and therefore eigenvalues  $\epsilon_m$  have real and imaginary parts, the real part being the quasiparticle energy  $E_m^{QP}$  and the imaginary part being related to the quasiparticle lifetime. In this

work the self-energy operator was computed within the *GW* approximation,<sup>10</sup> in which the self-energy operator is obtained from convolution of the noninteracting single-particle Green's function  $G_0$  and the screened Coulomb interaction  $W$

$$\Sigma(\mathbf{r}, \mathbf{r}', E) = \frac{i}{2\pi} \int e^{-i\omega 0^+} G_0(\mathbf{r}, \mathbf{r}', E - \omega) W(\mathbf{r}, \mathbf{r}', \omega) d\omega. \quad (2)$$

$G_0$  is constructed from DFT single-particle orbitals  $\psi_n^{SP}$  and eigenvalues  $E_n^{SP}$  of the Kohn-Sham operator

$$G_0(\mathbf{r}, \mathbf{r}', \omega) = \sum_n \frac{\psi_n^{SP}(\mathbf{r}) \psi_n^{*SP}(\mathbf{r}')}{\omega - E_n^{SP} + i0^+ \text{sign}(E_n^{SP} - E_F)}. \quad (3)$$

For light elements it has been found that quasiparticle amplitudes are well approximated by DFT wave functions.<sup>12</sup> Thus, quasiparticle energies are simply given by

$$E_{mk}^{QP} = E_{mk}^{SP} + \langle \psi_{mk}^{SP} | \Sigma(E_{mk}^{QP}) - V_{xc}[n_v] | \psi_{mk}^{SP} \rangle. \quad (4)$$

In this case only diagonal elements of the self-energy matrix and exchange-correlation potential  $V_{xc}[n_v]$  are required.  $V_{xc}[n_v]$  is the exchange-correlation potential of the valence electron density  $n_v$  from the initial DFT calculation. Equation (4) is solved using a scheme given by Hybertsen and Louie.<sup>12</sup> For convenience later on we define the operator  $\Delta\Sigma$  to be  $\Delta\Sigma(\mathbf{r}, \mathbf{r}', E) = \Sigma(\mathbf{r}, \mathbf{r}', E) - V_{xc}[n_v]$ .

### B. Self-energy matrix elements

The screened Coulomb interaction is computed from the dielectric function and the bare Coulomb interaction

$$W(\mathbf{r}, \mathbf{r}', \omega) = \int \epsilon^{-1}(\mathbf{r}, \mathbf{r}'', \omega) v(\mathbf{r}'', \mathbf{r}') d\mathbf{r}''. \quad (5)$$

Two-point functions in a crystal lattice, such as the screened interaction, have the property  $f(\mathbf{r} + \mathbf{R}, \mathbf{r}' + \mathbf{R}) = f(\mathbf{r}, \mathbf{r}')$ , where  $\mathbf{R}$  is a Bravais lattice vector, owing to translational symmetry. They may be represented as a Fourier transform as,<sup>12</sup>

$$f(\mathbf{r}, \mathbf{r}') = \sum_{\mathbf{q}, G, G'} e^{i(\mathbf{q} + \mathbf{G}) \cdot \mathbf{r}} f_{GG'}(\mathbf{q}) e^{-i(\mathbf{q} + \mathbf{G}') \cdot \mathbf{r}'}, \quad (6)$$

where  $\mathbf{G}$  is a reciprocal lattice vector and  $\mathbf{q}$  is a wave vector in the first Brillouin zone. Fourier coefficients of the screened potential  $W_{GG'}$  are given by

$$W_{GG'}(\mathbf{q}, \omega) = \frac{4\pi e^2}{\Omega} \frac{1}{|\mathbf{q} + \mathbf{G}| |\mathbf{q} + \mathbf{G}'|} \epsilon_{GG'}^{-1}(\mathbf{q}, \omega), \quad (7)$$

where  $\Omega$  is the crystal volume and  $\epsilon_{GG'}^{-1}$  is the inverted, symmetrized RPA dielectric matrix. Numerical evaluation of  $W$  and  $\Sigma$  [Eqs. (2) and (7)] requires calculation and inversion of the dielectric matrix at many values of  $\omega$ . Such schemes have been carried out within PP (Ref. 27) and all electron calculations.<sup>26</sup> Here, however, the screened interaction  $W$  is approximated using a plasmon-pole model, and the integral in Eq. (2) is evaluated analytically. This is applicable for simple systems with only *s*- and *p*-type orbitals occupied, such as Ne and Ar. The main shortcoming of the plasmon-pole model is that it is not suitable for accurate calculation of self-energy matrix elements of high energy bands. However this will not be a major concern here since we are mainly interested in valence bands and the lowest conduction bands for excitonic optical spectra calculations.<sup>14</sup> We adopt a plasmon-pole model based on the work of von der Linden and Horsch,<sup>28</sup> which uses the concept of dielectric band structure<sup>29</sup> to approximate the frequency dependence of the dielectric matrix. The model assumes that all frequency dependence is projected onto eigenvalues of the inverted dielectric matrix,  $\epsilon_{q_l}^{-1}(\omega)$  through the approximation,

$$\epsilon_{q_l}^{-1}(\omega) = 1 + \frac{z_{q_l} \omega_{q_l}}{2} \left( \frac{1}{\omega - \omega_{q_l} + i0^+} - \frac{1}{\omega + \omega_{q_l} - i0^+} \right). \quad (8)$$

$z_{q_l}$  are pole strengths,  $\omega_{q_l}$  are plasmon frequencies, and  $0^+$  is a positive infinitesimal. Eigenvalues of the inverted dielectric matrix determine the pole strengths, and a plot of their dispersion with wave vector is known as the dielectric band structure;<sup>29</sup> the dielectric band structure for fcc Ar was reported previously.<sup>30</sup> Plasmon pole frequencies are calculated using the Johnson sum rule.<sup>31</sup> This leads to two contributions to the self-energy: an energy independent, Hartree-Fock exchange term,

$$\langle mk | \Sigma_x | mk \rangle = - \frac{4\pi e^2}{\Omega} \sum_{\mathbf{q}, G} \sum_n^{occ} \frac{|\langle mk | e^{-i(\mathbf{q} + \mathbf{G}) \cdot \mathbf{r}} | nk + \mathbf{q} \rangle|^2}{|\mathbf{q} + \mathbf{G}|^2}, \quad (9)$$

where the sum over bands  $n$  extends only over occupied states. The second, dynamic part

$$\begin{aligned} \langle mk | \Sigma_c(E) | mk \rangle &= \frac{4\pi e^2}{\Omega} \sum_{\mathbf{q}, G, G'} \sum_n^{occ} \frac{\langle mk | e^{-i(\mathbf{q} + \mathbf{G}) \cdot \mathbf{r}} | nk + \mathbf{q} \rangle \langle nk + \mathbf{q} | e^{i(\mathbf{q} + \mathbf{G}') \cdot \mathbf{r}'} | mk \rangle}{|\mathbf{q} + \mathbf{G}| |\mathbf{q} + \mathbf{G}'|} \\ &\quad \times \sum_l V_{l, -G}(-\mathbf{q}) V_{l, -G'}^*(-\mathbf{q}) \left[ \frac{z_{-q_l} \omega_{-q_l}}{2} \frac{1}{E - E_{nk+\mathbf{q}} + \omega_{-q_l} \text{sign}(E_F - E_{nk})} \right], \end{aligned} \quad (10)$$

contains correlation energies of electron or hole quasiparticles.<sup>32</sup>  $V_{l, -G}$  are eigenvectors of the static, symmetrized dielectric matrix  $\epsilon_{GG'}(\mathbf{q}, \omega=0)$ .

TABLE I. DFT and *GW* data for different all electron basis sets. The row labeled AO indicates the number of atomic orbitals (AO) in the basis set.

	DFT (eV)			GW (eV)		
Neon						
AO	44	48	53	44	48	53
$\Gamma_{15v}$	-13.16	-13.16	-13.18	-19.05	-19.05	-19.07
$\Gamma_{1c}$	-1.16	-1.41	-1.42	1.37	1.01	0.97
$W_v$	0.69	0.69	0.79	0.91	0.91	0.91
$E_g$	12.00	11.75	11.76	20.42	20.07	20.13
Argon						
AO	57	61	66	57	61	66
$\Gamma_{15v}$	-10.12	-10.14	-10.27	-12.91	-12.92	-13.02
$\Gamma_{1c}$	-0.16	-0.64	-0.76	1.62	0.96	0.80
$W_v$	1.31	1.32	1.32	1.80	1.82	1.83
$E_g$	9.96	9.50	9.51	14.54	13.89	13.82

### C. Numerical details

The starting point in our approach is to generate noninteracting single-particle Green's functions of an  $N$ -electron system. We use density functional theory<sup>33</sup> (DFT) within the Perdew-Wang generalized gradient approximation<sup>34</sup> (PWGGA) to obtain eigenvectors and eigenvalues of the Kohn-Sham Hamiltonian. For this part of the calculation we employ the *ab initio* package CRYSTAL,<sup>16</sup> which uses the linear-combination-of-atomic-orbitals (LCAO) approach to expand the Bloch functions. In order to investigate convergence criteria within the Gaussian orbital framework and effects of core electrons, we performed both all electron and PP calculations for each solid. Basis sets with 52 and 53 functions per atom were developed for PP and all electron calculations, respectively, for Ne. The PP and all electron basis sets for Ar contained 56 and 66 functions, respectively. Details of basis sets are given in the Appendix. Pseudopotentials from Barthelat *et al.*<sup>35</sup> were used in PP calculations. Experimental lattice constants<sup>36</sup> were used. Convergence of results with respect to basis set was investigated by developing several smaller basis sets. Positions of valence-band maximum ( $\Gamma_{15v}$ ) and conduction-band minimum states ( $\Gamma_{1c}$ ), valence bandwidths,  $W_v$  and band gaps,  $E_g$ , were evaluated using several basis sets and results are given in Table I. The most sensitive dependence on the choice of basis set is the conduction-band minimum position in *GW* calculations. However the difference in that level for the largest (53 AO) and smallest (44 AO) basis sets for Ne is only 0.04 eV. The conduction-band minimum for Ar differs by 0.16 eV between the 66 AO and 61 AO basis sets, but the difference in the fundamental gap is  $<0.1$  eV for these two basis sets, which suggests that the 66 AO basis set converges the band-gap well. The valence bandwidth is well converged in all *GW* and DFT calculations. The sum over  $\mathbf{q}$  points in Eqs. (9) and (10) as well as integration over the Brillouin zone in the dielectric matrix calculation is performed using Monkhorst-Pack<sup>37</sup> special points. The singularity in Eqs. (9) and (10) of  $1/q^2$  type for  $\mathbf{q} \rightarrow 0$  and  $\mathbf{G}=\mathbf{G}'=0$  was integrated out using the auxiliary function technique of Gygi and

Baldereschi,<sup>38</sup> while the singularity in Eq. (10) of  $1/q$  type was neglected since the final result is not affected if it is neglected.<sup>21</sup> Two special points in the irreducible Brillouin zone were used for calculation of self-energy matrix elements and an  $8 \times 8 \times 8$  grid in the full Brillouin zone was used for the dielectric matrix calculation. Up to 400 (8000)  $\mathbf{G}$  vectors are required to achieve convergence of the Hartree-Fock part of the self-energy [Eq. (9)] for PP (all electron) basis sets for second row elements. In the summation over  $\mathbf{G}$  and  $\mathbf{G}'$  vectors in Eq. (10), 65 vectors gave well converged results for all solids.

### D. Core-valence exchange-correlation decoupling

When matrix elements of the  $\Delta\Sigma$  operator are evaluated, contributions from core electrons to the valence electron self-energy must be considered.<sup>11,12</sup> We compare results from two alternative approximations for the energy independent part of the  $\Delta\Sigma$  operator, which were applied recently in all electron *GW* calculations on Si.<sup>21</sup> The first approximation is to compute matrix elements of the DFT exchange-correlation potential using the valence electron density only and to restrict the sum on occupied states in Eq. (9) to valence states only,

$$\langle m\mathbf{k}|\Delta\Sigma|m\mathbf{k}\rangle = \langle m\mathbf{k}|\Sigma_c^{\text{val}}|m\mathbf{k}\rangle + \langle m\mathbf{k}|\Sigma_x^{\text{val}}|m\mathbf{k}\rangle - \langle m\mathbf{k}|V_{xc}[n_v]|m\mathbf{k}\rangle. \quad (11)$$

The second approximation is to replace matrix elements of the valence-density-only exchange correlation potential,  $V_{xc}[n_v]$ , in Eq. (11) by

$$\langle m\mathbf{k}|V_{xc}[n_c + n_v]|m\mathbf{k}\rangle - \langle m\mathbf{k}|\Sigma_x^{\text{core}}|m\mathbf{k}\rangle. \quad (12)$$

The notation  $\langle m\mathbf{k}|\Sigma_x^{\text{core}}|m\mathbf{k}\rangle$  and  $\langle m\mathbf{k}|\Sigma_x^{\text{val}}|m\mathbf{k}\rangle$  indicates that the sum on  $n$  in Eq. (9) is limited to core or valence states only. Matrix elements of the LDA exchange potential and Hartree-Fock exchange operator for valence-band maximum and conduction-band minimum states in silicon obtained by Arnaud and Alouani<sup>21</sup> using a projector augmented wave (PAW) method and in this work using CRYSTAL are compared

TABLE II. Matrix elements of the Hartree-Fock exchange ( $\Sigma_x$ ) and LDA exchange potential ( $V_x$ ) operators for self-consistent DFT wave functions at valence-band maxima and conduction-band minima for Si. The symbols  $n_c+n_v$ , core, and  $n_v$  denote whether core plus valence, core-only, or valence-only states are included in the operators.

	$V_x[n_c+n_v]$	$\Sigma_x^{\text{core}}$	$V_x[n_v]$
$\Gamma_{15c}^a$	-11.75	-1.32	-10.18
$\Gamma_{15c}^b$	-11.74	-1.40	-10.19
$\Gamma_{25'v}^a$	-13.55	-1.80	-11.45
$\Gamma_{25'v}^b$	-13.45	-1.85	-11.46

<sup>a</sup>This work.

<sup>b</sup>Reference 21.

in Table II. Remarkably good agreement was found between LDA exchange potential matrix elements from either method (differences in matrix elements are only 0.01 eV in three out of four cases) and good agreement between Hartree-Fock exchange matrix elements is also obtained (within 0.1 eV). The shortcoming of the latter approach [Eq. (12)] is slow convergence of the Hartree-Fock exchange operator for core states,  $\langle m\mathbf{k}|\Sigma_x^{\text{core}}|m\mathbf{k}\rangle$ .

### III. RESULTS AND DISCUSSION

One of the aims of this work is to compare results of *GW* calculations on simple atomic solids which treat core electrons either by a PP or by explicitly including them in an all electron calculation. Energies of states at valence-band maxima and conduction-band minima are given in Table III, as well as fundamental band gaps and valence bandwidths within DFT and *GW* approximations and experiment. *GW* all electron quasiparticle energies obtained by the two core-valence electron decoupling methods outlined in Eqs. (11) and (12) are given in columns labeled  $E_{(1)}^{QP}$  and  $E_{(2)}^{QP}$ . DFT-PP calculations underestimate experimental band gaps by 45%

for Ne and by 35% for Ar. *GW*-PP calculations show significantly improved agreement with experimental data in each solid; the band-gap error is reduced to 6% in Ne and 2% in Ar; slight underestimation of band-gaps in RGS is similar to that in semiconductors where a plasmon pole approximation has been applied. For example, the band gap is underestimated by 4% in Si.<sup>39</sup> The reason for good agreement between quasiparticle energies,  $E_1^{QP}$  and  $E_2^{QP}$ , for Ne and Ar (this work) and Si<sup>21</sup> is that the energy-independent part of the  $\Delta\Sigma$  operator is  $\Sigma_x^{\text{val}} - V_{xc}[n_v]$  for  $E_1^{QP}$  and it is  $\Sigma_x^{\text{core+val}} - V_{xc}[n_c+n_v]$  for  $E_2^{QP}$ ; the difference in these two quantities is of order 0.1 eV and results in nearly equal quasiparticle energies,  $E_1^{QP}$  and  $E_2^{QP}$ . There is good agreement between PP and all electron DFT calculations for Ne; the bottom conduction ( $\Gamma_{15v}$ ) and top valence band ( $\Gamma_{1c}$ ) energies and valence bandwidths ( $W_v$ ) differ by less than 0.1 eV.  $\Gamma_{15v}$  and  $\Gamma_{1c}$  quasiparticle energies from all electron calculations lie slightly above PP values. The absolute value of the  $\Gamma_{1c}$  conduction-band energy, which determines the electron affinity, has the correct sign in *GW* calculations and lies just 0.4 eV below the experimental value for the electron affinity, whereas DFT calculations predict larger electron affinities of the wrong sign. *GW* calculations result in valence band-

TABLE III. DFT eigenvalues and *GW* quasiparticle energies at valence-band maxima and conduction-band minima, valence bandwidths, and energy gaps for Ne and Ar RGS. Calculations were performed using pseudopotentials (second and third columns) and all electron basis sets (fourth to sixth columns). The fifth column,  $E_{(1)}^{QP}$  gives all electron *GW* data when  $V_{xc}[n_v]$  is calculated explicitly [Eq. (11)] and the sixth column gives quasiparticle energies when  $V_{xc}[n_v]$  is calculated using Eq. (12). The last column gives experimental data. Experimental data is taken from Ref. 17 unless cited differently. Energies are given in electron volts (eV).

	PP		All-electron			Exp.
	DFT	$E^{QP}$	DFT	$E_{(1)}^{QP}$	$E_{(2)}^{QP}$	
Neon						
$\Gamma_{15v}$	-13.14	-19.37	-13.18	-19.07	-19.10	-20.21
$\Gamma_{1c}$	-1.35	0.86	-1.42	0.97	1.03	1.3
$W_v$	0.71	0.93	0.79	0.91	0.93	1.3 <sup>a</sup>
$E_g$	11.99	20.23	11.76	20.04	20.13	21.51
Argon						
$\Gamma_{15v}$	-9.74	-13.15	-10.27	-13.02	-13.00	-13.75
$\Gamma_{1c}$	-0.60	0.72	-0.76	0.80	0.81	0.4
$W_v$	1.35	1.73	1.32	1.83	1.85	1.7 <sup>a</sup>
$E_g$	9.13	13.89	9.51	13.82	13.81	14.15

<sup>a</sup>Reference 19.

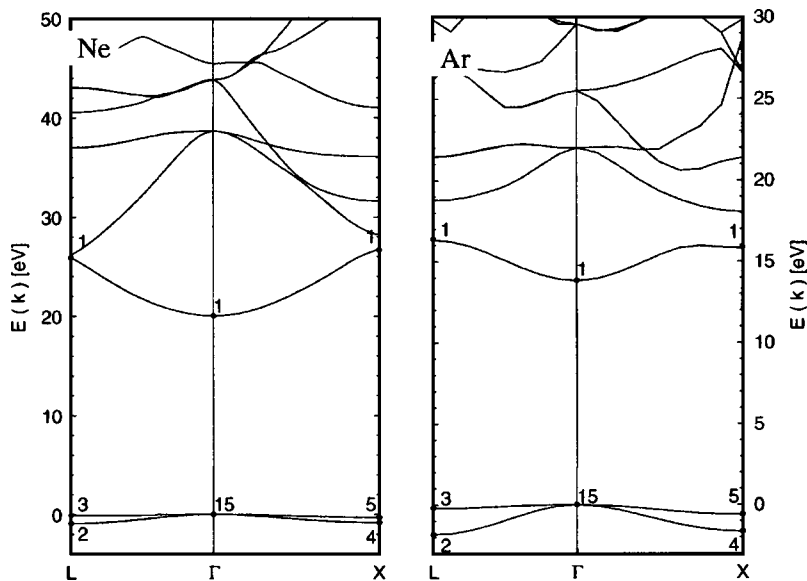


FIG. 1. GW band structure for Ne (left panel) and Ar (right panel).

widths  $\sim 0.9$  eV, which are smaller than the experimental value of 1.3 eV,<sup>19</sup> but are in agreement with the value of 0.99 eV obtained by Bacalis *et al.*<sup>2</sup> The two methods used for core-valence decoupling (Table III, columns 5 and 6) result in  $\Gamma_{15v}$  and  $\Gamma_{1c}$  quasiparticle energies which differ by only  $\sim 0.05$  eV.

The  $\Gamma_{15v}$  valence-band maximum state in all electron DFT calculations on Ar is lower than in PP calculations by 0.53 eV, whereas the  $\Gamma_{1c}$  conduction-band minimum state is lower by 0.16 eV. However GW quasiparticle energies for these states using either all electron or PP basis sets are in good agreement, the maximum difference being only 0.13 eV. The GW  $\Gamma_{1c}$  conduction-band energy exceeds the experimental electron affinity by  $\sim 0.4$  eV, whereas the DFT  $\Gamma_{1c}$  energy again predicts an electron affinity with the wrong sign. GW valence bandwidths of 1.73 (PP) and 1.83 eV (all electron) agree very well with the experimental value of

1.7 eV.<sup>19</sup> The two methods used for core-valence decoupling also result in very similar quasiparticle energies for Ar.

GW band structures along  $\Delta$  and  $\Sigma$  symmetry lines for Ne and Ar are shown in Fig. 1. Self-energy corrections to GW band structures in both Ne and Ar are relatively independent of wave vector, leading to a *scissor*-type opening of the band gap on going from DFT to GW energy bands. DFT band structures are not shown in Fig. 1 for clarity. Tables IV and V give a direct comparison of all electron DFT energy eigenvalues and GW quasiparticle energies at high-symmetry points for Ne and Ar and include results from Bacalis *et al.*<sup>2</sup> and experiment. The band gap for Ne from a DFT calculation that used the PWGGA functional (this work) is in good agreement with the value reported by Bacalis *et al.*<sup>2</sup> for Ne; however, the band gap of 9.51 eV for Ar exceeds the value of 8.09 eV from Bacalis *et al.*,<sup>2</sup> significantly. The major difference between our calculation and that in Ref. 2 is use of

TABLE IV. Energy eigenvalues in electron volts at high-symmetry points for solid Ne. The reference energy is the valence-band maximum energy. Results in the second and third columns were obtained using an all electron basis set and valence-core electron decoupling was done using the method outlined in Eq. (11). Results in the fourth and fifth columns are from all electron projector augmented wave (PAW) calculations.<sup>2</sup> The last column presents experimental values.

	This work		PAW <sup>a</sup>		Exp.
	DFT	GW	DFT	GW	
$\Gamma_{15v}$	0.0	0.0	0.0	0.0	0.0
$\Gamma_{1c}$	11.76	20.04	11.40	16.56	21.51 <sup>b</sup>
$X'_{4v}$	-0.61	-0.82	-0.67	-0.88	
$X'_{5v}$	-0.21	-0.29	-0.23	-0.30	
$L'_{2v}$	-0.69	-0.91	-0.75	-0.99	-1.3 <sup>c</sup>
$L'_{3v}$	-0.07	-0.10	-0.07	-0.09	
$\Gamma'_{25c}-\Gamma_{1c}$	17.85	18.57	18.12	20.51	
$X_{1c}-\Gamma_{1c}$	6.78	6.66	6.82	8.12	
$L_{1c}-\Gamma_{1c}$	5.57	5.91	6.03	7.21	

<sup>a</sup>Reference 2.

<sup>b</sup>Reference 17.

<sup>c</sup>Reference 19.

TABLE V. Energy eigenvalues in electron volts at high-symmetry points for solid Ar. The reference energy is the valence-band maximum energy. Results in the second and third columns were obtained using an all electron basis set and valence-core electron decoupling was done using the method outlined in Eq. (11). Results in the fourth and fifth columns are from all electron PAW calculations.<sup>2</sup> The last column presents experimental values.

	This work		PAW <sup>a</sup>		Exp.
	DFT	GW	DFT	GW	
$\Gamma_{15v}$	0.0	0.0	0.0	0.0	0.0
$\Gamma_{1c}$	9.51	13.82	8.09	11.96	14.15 <sup>b</sup>
$X'_{4v}$	-1.19	-1.65	-1.28	-1.73	
$X'_{5v}$	-0.42	-0.50	-0.46	-0.63	
$L'_{2v}$	-1.31	-1.83	-1.41	-1.92	-1.7 <sup>c</sup>
$L'_{3v}$	-0.14	-0.20	-0.16	-0.20	
$\Gamma'_{25c}-\Gamma_1$	6.85	8.21	7.43	8.44	
$X_{1c}-\Gamma_{1c}$	2.02	2.04	2.63	3.10	
$L_{1c}-\Gamma_{1c}$	2.25	2.56	2.94	3.50	

<sup>a</sup>Reference 2.

<sup>b</sup>Reference 17.

<sup>c</sup>Reference 19.

the PWGGA functional in this work, while the LDA was used in the latter. Replacing the PWGGA by the LDA in our calculation, the valence-band maximum shifts from -10.27 eV (see Table III) to -9.23 eV, while the conduction bands were nearly unaffected, leading to lowering of the band gap from 9.51 eV to 8.55 eV, which agrees reasonably well with value of 8.09 eV obtained by Bacalis *et al.*<sup>2</sup> When DFT and quasiparticle energies for Ne at  $X$  and  $L$  points are compared (Table IV), we find a widening of the valence bands by approximately 30%. Our results for valence band energies and widths are in very good agreement with those reported earlier by Bacalis *et al.*<sup>2</sup> A similar pattern of valence band widening for  $GW$  valence bands in Ne is found in Ar, and our results are again in good agreement with those of Bacalis *et al.*<sup>2</sup> The energy difference of the first and second conduction bands at the  $\Gamma$  point ( $\Gamma_{25c'}-\Gamma_{1c}$ ) in our  $GW$  calculation is  $\sim 2$  eV smaller than in the projector augmented wave (PAW)<sup>2</sup> calculation for Ne, while the value of 8.21 eV for Ar agrees well with the value of 8.44 eV obtained by Bacalis *et al.* This energy difference is sensitive to completeness of Gaussian orbital basis sets (see the Appendix) as the  $\Gamma_{25c'}$  state has significant amplitude in octahedral interstitial regions. Inclusion of interstitial functions in basis sets (Appendix) and optimization of the most diffuse functions reduced the  $\Gamma_{25c'}-\Gamma_{1c}$  energy difference significantly, while basis sets with no interstitial functions result in a larger conduction band separation and fundamental gap.

#### IV. CONCLUSIONS

Band structures of solid Ne and Ar have been calculated using the  $GW$  approximation. Calculations were performed using experimental lattice constants. Gaussian orbital basis sets were used throughout and core electrons were treated either explicitly with all electron basis sets or by pseudopotentials. Results of all electron and pseudopotential calcula-

tions are in good agreement, although the fundamental band gap predicted by all electron calculations is smaller than that in pseudopotential calculations by up to 0.2 eV. Positions of conduction band minima for Ne and Ar in  $GW$  calculations are in good agreement with experimental electron affinities so that absolute positions of quasiparticle energy levels in Ne and Ar are reliably predicted in the  $GW$  approximation. Fundamental band gaps for Ne and Ar are in good agreement with experimental gaps from photoemission and optical absorption data where shifts in the gap due to electron-hole attraction have been subtracted.

#### ACKNOWLEDGMENTS

This work was supported by Enterprise-Ireland under Grant No. SC/99/267 and by the Irish Higher Education Authority under the PRTLII-IITAC2 program. C.H.P. wishes to thank R. Dovesi and C. Roetti for hospitality during a visit to the Università di Torino, which was supported by the Royal Irish Academy.

#### APPENDIX: BASIS SETS

The construction and use of an appropriate basis set constitutes a critical factor in *ab initio* calculations and is particularly important within a Gaussian orbital framework. Apart from minimizing the total energy, which is necessary for a good quality basis set, one has to ensure that the basis set contains a sufficient number of basis functions to generate the virtual space. The need for a large number of conduction bands for a well-converged self-energy has been emphasized again recently.<sup>25</sup> The number of conduction bands can be increased by including  $f$ - and  $g$ -type functions into the basis set, but these are not yet available in the CRYSTAL code. Alternatively, extra sets of orbitals were added at interstitial sites of the crystal. This improves the flexibility of the basis

TABLE VI. Basis sets used in this work. Exponents of  $s$ ,  $p$ , and  $d$  Cartesian Gaussian orbitals, which were centered on the nuclear site [(0,0,0) labeled Nuc.] and at the octahedral interstitial site of the fcc lattice [(0.5,0.5,0.5) labeled Oct.] are tabulated in atomic units. Basis sets for atomic cores in all electron calculations were conventional quantum chemistry core basis sets and are not given here.

Ne							
Nuc. sp	32.0	16.0	4.0	2.0	1.4	0.47	0.185
Nuc. d					1.6	0.8	0.2
Oct. sp							0.3
Oct. d							0.3
Ar-Basis set 1							
Nuc. sp	32.0	16.0	4.0	2.0	1.4	0.47	0.15
Nuc. d					0.8	0.4	0.2
Oct. sp						0.47	0.15
Oct. d							0.4
Ar-Basis set 2							
Nuc. sp	85.0	34.0	14.0	1.4	0.8	0.39	0.2
Nuc. d				1.05	0.79	0.39	0.1
Oct. sp						0.61	0.31
Oct d							0.2

set through the unit cell and attempts to reproduce the highly nodal structure of free-electron conduction band states.

Two techniques were used for constructing basis sets: First, starting from two decay constants, 0.15 and 2.0, geometrical expansion was used to generate more localized orbitals, interstitial functions were added and the most diffuse functions were adjusted to minimize the total energy. The second approach used valence exponents from conventional, contracted quantum chemistry basis sets. Several Gaussian

functions are combined into a single basis function in a contracted basis function by fixing their weights. Here the same exponents as used in contracted basis functions were used, but relative weights of different exponents were determined during the self-consistent field DFT calculation. The basis set used for PP Ne and Ar (Basis set 1) and all electron Ne calculations was of the first type, while all electron Ar calculations were performed using a basis set of the second type (Basis set 2). These are shown in Table VI.

<sup>1</sup>N. O. Lipari and W. B. Fowler, Phys. Rev. B **2**, 3354 (1970).

<sup>2</sup>N. C. Bacalis, D. A. Papaconstantopoulos, and W. E. Pickett, Phys. Rev. B **38**, 6218 (1988).

<sup>3</sup>R. J. Magyar, A. Fleszar, and E. K. U. Gross, Phys. Rev. B **69**, 045111 (2004).

<sup>4</sup>L. Dagens and F. Perrot, Phys. Rev. B **5**, 641 (1972).

<sup>5</sup>A. B. Kunz and D. J. Mickish, Phys. Rev. B **8**, 779 (1973).

<sup>6</sup>S. Baroni, G. Grosso, and G. Pastori Parravicini, Phys. Rev. B **23**, 6441 (1981).

<sup>7</sup>S. Baroni, G. Grosso, and G. Pastori Parravicini, Phys. Rev. B **29**, 2891 (1984).

<sup>8</sup>R. A. Heaton, J. Harrison, and C. Lin, Phys. Rev. B **28**, 5992 (1983).

<sup>9</sup>M. Rohlfing and S. G. Louie, Phys. Rev. B **62**, 4927 (2000).

<sup>10</sup>L. Hedin, Phys. Rev. **139**, A796 (1965).

<sup>11</sup>L. Hedin and L. Lundqvist, *Solid State Physics* (Academic Press, New York, 1969), Vol. 23.

<sup>12</sup>M. S. Hybertsen and S. G. Louie, Phys. Rev. B **34**, 5390 (1986).

<sup>13</sup>F. Aryasetiawan and O. Gunnarsson, Rep. Prog. Phys. **61**, 237 (1998).

<sup>14</sup>S. Galamić-Mulaomerović and C. H. Patterson (unpublished).

<sup>15</sup>S. Galamić-Mulaomerović, C. D. Hogan, and C. H. Patterson (unpublished).

<sup>16</sup>V. R. Saunders, R. Dovesi, C. Roetti, M. Causá, R. Orlando, C.

M. Zicovich-Wilson, N. M. Harrison, K. Doll, B. Civalieri, I. Bush *et al.*, *CRYSTAL03 User's Manual*, Torino, 2003.

<sup>17</sup>M. Runne and G. Zimmerer, Nucl. Instrum. Methods Phys. Res. B **101**, 156 (1995).

<sup>18</sup>N. Schwentner, M. Skibowski, and W. Steinmann, Phys. Rev. B **8**, 2965 (1973).

<sup>19</sup>N. Schwentner, F.-J. Himpsel, V. Savle, M. Skibowski, W. Steinmann, and E. Koch, Phys. Rev. Lett. **34**, 528 (1975).

<sup>20</sup>N. Hamada, M. Hwang, and A. J. Freeman, Phys. Rev. B **41**, 3620 (1990).

<sup>21</sup>B. Arnaud and M. Alouani, Phys. Rev. B **62**, 4464 (2000).

<sup>22</sup>T. Kotani and M. van Schilfgarde, Solid State Commun. **121**, 461 (2002).

<sup>23</sup>W. Ku and A. G. Eguiluz, Phys. Rev. Lett. **89**, 126401 (2002).

<sup>24</sup>S. V. Faleev, M. van Schilfgarde, and T. Kotani, Phys. Rev. Lett. **93**, 126406 (2004).

<sup>25</sup>M. L. Tiago, S. Ismail-Beigi, and S. G. Louie, Phys. Rev. B **69**, 125212 (2004).

<sup>26</sup>S. Lebègue, B. Arnaud, M. Alouani, and P. E. Bloechl, Phys. Rev. B **67**, 155208 (2003).

<sup>27</sup>R. W. Godby, M. Schlüter, and L. J. Sham, Phys. Rev. B **37**, 10 159 (1988).

<sup>28</sup>W. von der Linden and P. Horsch, Phys. Rev. B **37**, 8351 (1988).

<sup>29</sup>A. Baldereschi and E. Tosatti, Solid State Commun. **29**, 131

- (1979).
- <sup>30</sup>S. Galamić-Mulaomerović, C. D. Hogan, and C. H. Patterson, *Phys. Status Solidi A* **188**, 1291 (2001).
- <sup>31</sup>D. L. Johnson, *Phys. Rev. B* **9**, 4475 (1974).
- <sup>32</sup>R. Hott, *Phys. Rev. B* **44**, 1057 (1991).
- <sup>33</sup>P. Hohenberg and W. Kohn, *Phys. Rev.* **136**, B864 (1964).
- <sup>34</sup>J. P. Perdew and Y. Wang, *Phys. Rev. B* **45**, 13 244 (1992).
- <sup>35</sup>J. Barthelat, P. Durand, and A. Serafini, *Mol. Phys.* **33**, 159 (1977).
- <sup>36</sup>B. Sonntag, in *Rare Gas Solids*, edited by M. L. Klein and J. A. Venables (Academic Press, London, 1977), Vol. 2.
- <sup>37</sup>H. J. Monkhorst and J. D. Pack, *Phys. Rev. B* **13**, 5188 (1976).
- <sup>38</sup>F. Gygi and A. Baldereschi, *Phys. Rev. B* **34**, R4405 (1986).
- <sup>39</sup>E. L. Shirley, X. Zhu, and S. G. Louie, *Phys. Rev. B* **56**, 6648 (1997).